Physics Letters A 376 (2012) 650–655

Contents lists available at SciVerse ScienceDirect

Physics Letters A

www.elsevier.com/locate/pla

Cold matter trapping via slowly rotating helical potential

A.Yu. Okulov *

Russian Academy of Sciences, 119991, Moscow, Russia

ARTICLE INFO

Keywords:
Superfluid hydrodynamics
Optical dipole traps
Angular momentum of vortices
Macroscopic many-body wavefunction

ABSTRACT

We consider the cold bosonic ensemble trapped by a helical interference pattern in the optical *loop* scheme. This rotating helical potential is produced by the two slightly detuned counter-propagating Laguerre–Gaussian laser beams with counter-directed orbital angular momenta $\pm\ell\hbar$. The detuning $\delta\omega$ may occur due to rotational Doppler effect. The superfluid hydrodynamics is analyzed for the large number of trapped atoms in Thomas–Fermi approximation. For the highly elongated trap the Gross–Pitaevskii equation is solved in a slowly varying envelope approximation. The speed of axial translation and angular momenta of interacting atomic cloud are evaluated. In the $T \to 0$ limit the angular momentum of the helical cloud is expected to be zero while toroidal trapping geometry leads to $2\ell\hbar$ angular momentum per trapped atom.

1. Introduction

The hydrodynamics of the sufficiently cold ($T \sim 10^{-6}$ K) bosonic ensemble trapped by optical potential $V(\vec{r},t)$ [1–3] is described by the Gross–Pitaevskii equation (GPE) [4] for macroscopic wavefunction $\Psi(\vec{r},t)$:

$$i\hbar\frac{\partial\Psi}{\partial t} = -\frac{\hbar^2}{2m}\Delta\Psi + V(\vec{r},t)\Psi + \frac{4\pi\hbar^2 a_s}{m}|\Psi|^2\Psi, \tag{1}$$

where m is the mass of atom, a_s is the two body s-wave scattering length. The negative a_s reduces the energy of ensemble and causes the mutual attraction of atoms. This results in formation of bright solitons in **1D** and collapse in higher dimensions. On the contrary in repulsive BECs atoms repel each other and dark solitons or vortices are formed. In the periodic potential gratings [5]:

$$V(\vec{r},t) \sim I(z,r,t) \sim \exp\left[-r^2\right]\cos\left[\delta\omega t - (k_f + k_b)z\right], \tag{2}$$

where r is a distance from propagation axis z, $\delta\omega = c\cdot(k_f - k_b) = \omega_f - \omega_b$ is a frequency difference of the counter-propagating z-paraxial laser beams with the opposite wave vectors $|\vec{k}_{(f,b)}| \approx k_{(f,b)}$, the many-body nonlinearity leads to the nonlinear tunneling, self-trapping and other quantum interference phenomena [6]. For accelerated **1D** optical gratings when $\delta\omega = \dot{\delta\omega}\cdot t$, i.e. in the noninertial reference frames [5] the interacting bosons demonstrate Bloch oscillations and Landau–Zener tunneling. In rotating **1D** lattices the repulsive ensemble may have stable ground states and vortex soliton states [7]. For the attractive ensemble in **2D** rotating lattices [8] the localized stable solitons exist in the certain range of angular velocities. Inside the parabolic well with trapping frequency $\omega_\perp$ and rotation frequency Ω the nonlinear localized matter waves appear when $\Omega \sim \omega_\perp$ at lowest Landau level [9] which appears due to the *fictionary magnetic field* induced by trap rotation [10].

The goal of the present work is to study bosonic ensemble in rotating reference frame by a virtue of rotating optical *dipole* trap whose rotation is due to the frequency detuning $\delta\omega$. The proposed trap configuration is composed of the two counter-propagating optical vortices. The shape of the interference pattern is defined by the mutual orientation of their orbital angular momenta $\pm\ell\hbar$ (OAM). When OAMs are co-directed the $\lambda/2$ spaced *toroidal* traps are formed by Laguerre–Gaussian (LG) [11] or Bessel vortices [12]. This geometry had been used for the single atom trapping and detection [13] and for the analysis of persistent condensate flows in LG beam waist [14]. When OAMs are counter-directed due to the phase-conjugation of the backward reflected LG beam the **1D** sinusoidal intensity grating is transformed into the truly **3D** *helicoidal* (Fig. 1, Section 2) grating $I(z,r,\theta,t)$ [11,12,15]. This grating experimentally observed for $\delta\omega = 0$ [16]:

$$I(z,r,\theta,t) \cong r^{2|\ell|}\exp\left[-r^2\right]\cos\left[\delta\omega t - (k_f + k_b)z + 2\ell\theta\right], \tag{3}$$

where z, r, θ are cylindrical coordinates, must rotate with angular frequency $\Omega = \dot{\theta} = \delta\omega/2\ell$ when $\delta\omega \neq 0$.

Noteworthy the similar interferometric configuration with counter-directed *spin* optical angular momenta (circular polarizations) which is used for the sub-Doppler polarization gradient cooling [17]. The interference pattern forms the static potential gratings due to Zeeman shift between ground-state sublevels. This

* Tel./fax: +7 495 382 4609.
E-mail address: alexey.okulov@gmail.com.

0375-9601/$ – see front matter
doi:10.1016/j.physleta.2011.11.033

causes the Sisyphus deceleration of the atomic beam in optical molasses.

We consider two possible regimes of the cold ensemble trapping when kinetic energy is small compared to the interaction and trapping energies. One Thomas–Fermi solution is obtained as a balance of the red-detuned optical attractive potential and self-defocussing due to positive a_s. This solution has atomic density ρ_h perfectly collocated with rotating optical helix $I(z,r,\theta,t)$. In this case the rotating potential imposes rotation to superfluid. The other TFA solution has nonrotating density "funnel" profile ρ_{fun} relevant to thermodynamic limit when number of atoms $N \to \infty$.

Next the analytical solution of GPE for nonzero kinetic energy Ψ_{hel} is described. It is valid when optical trapping and interaction energies are comparable and subtract each other in GPE. The linear momentum $\langle P_z \rangle$ and angular momentum $\langle L_z \rangle$ of this helical atomic cloud are evaluated. The Landau criterion $|\vec{V}| > \epsilon(\vec{p})/|\vec{p}|$ for the appearance of elementary excitations and superfluidity breakup [18] is discussed for helical geometry.

2. Twisted wavetrains

It is well known that interference of a two counter propagating waves with a different frequencies ω_f, ω_b produces a running sinusoidal *roll* intensity grating [6,19]. For the equal wave amplitudes $|\mathbf{E}_f|$, $|\mathbf{E}_b|$ and the phase difference ϕ the distribution of the light intensity $I(z,r,\theta,t)$ has the following form:

$$I(z,r,\theta,t) \sim 2|\mathbf{E}_{(f,b)}|^2\big[1+\cos\big[\delta\omega t-(k_f+k_b)z+\phi\big]\big] \times \exp\left[-\frac{r^2}{D_0{}^2(1+z^2/z_R^2)}\right], \quad z_R = k_{(f,b)}D_0{}^2, \quad (4)$$

provided that a visibility of pattern is good enough $|\mathbf{E}_{(f)}| \cong |\mathbf{E}_{(b)}|$ [20], where z_R is Rayleigh range, D_0 is a beam waist radius, the self-similar variable $\chi = (\omega_f-\omega_b)t-(k_f+k_b)z+\phi$ is responsible for the translation of the interference pattern along z-axis with the *group* velocity $V_z = (\omega_f-\omega_b)/(k_f+k_b)$. The transversal (in the plane (r,θ)) confinement of the light amplitudes $\mathbf{E}_f$, $\mathbf{E}_b$ is typical for the zeroth-order Gaussian beams. The *roll* interference pattern evolves into the sequence of the equidistantly spaced rotationally invariant in θ *ellipsoids* centered at the propagation axis z [11]. For the higher-order propagation modes namely Laguerre–Gaussian beams (LG) with azimuthal quantum number ℓ and orbital angular momentum $\ell\hbar$ per photon [21]:

$$\mathbf{E}_{(f,b)}(z,r,\theta,t) \sim \frac{\mathbf{E}_{(f,b)}\exp[i(-\omega_{(f,b)}t \pm k_{(f,b)}z) \pm i\ell\theta]}{(1+iz/z_R)}(r/D_0)^{|\ell|} \times \exp\left[-\frac{r^2}{D_0{}^2(1+iz/z_R)}\right], \quad (5)$$

the interference pattern is different for LG reflected from conventional mirror and phase-conjugating mirror. Backward reflection from conventional spherical mirror changes the topological charge of the LG [11], exactly in the same way as circular polarization of light changes from left to right and vice-versa in reflection [19]. The intensity $I_{tor}(z,r,\theta,t)$ vanishes on the beam axis thus interference pattern transforms into the sequence of the equidistant rotationally invariant *toroids* separated by $\lambda/2$ interval:

$$I_{tor}(z,r,\theta,t) = A_n\big[1+\cos\big[\delta\omega\cdot t-(k_f+k_b)z\big]\big](r/D_0)^{2|\ell|} \times \exp\left[-\frac{2r^2}{D_0{}^2(1+z^2/z_R^2)}\right],$$
$$A_n = \epsilon_0 c\frac{2|\mathbf{E}_{(f,b)}|^2 2^{(|\ell|+1)}}{\pi\,\ell!\,D_0{}^2}, \quad (6)$$

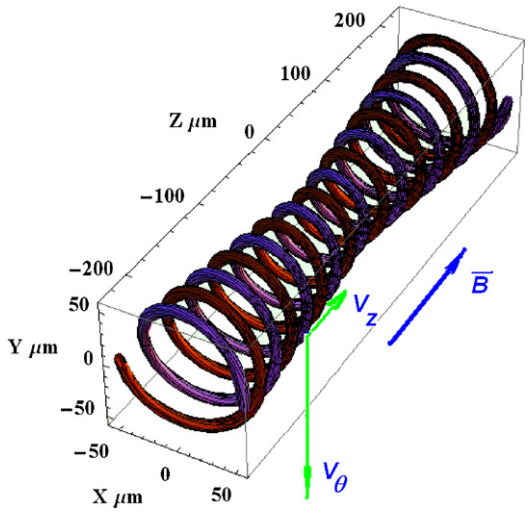

Fig. 1. The isosurface of the optical intensity I_{tw} and the Thomas–Fermi density ρ_h of the cold atomic cloud in a helical optical dipole trap (7), (19) (the scales are in μm, but longitudinal modulation of $\lambda/2$ is enlarged). The spatial modulation is induced by the interference of counter-propagating LG beams with the opposite angular momenta. The pattern rotates with angular frequency $\delta\omega/2\ell$ as a "solid body". Magnetic field $\vec{\mathbf{B}}$ adjusts the scattering length a_s to balance the attractive optical potential by many-body defocussing.

where ϵ_0 is the dielectric permittivity of vacuum. The reflection from phase-conjugating mirror (PCM) does not change the topological charge of LG and the interference pattern is twisted [11,16]:

$$I_{tw}(z,r,\theta,t) = \big[1+\cos\big[\delta\omega\cdot t-(k_f+k_b)z+2\ell\theta\big]\big]A_n \cdot (r/D_0)^{2|\ell|}\exp\left[-\frac{2r^2}{D_0{}^2(1+z^2/z_R^2)}\right]. \quad (7)$$

The intensity also vanishes at LG axis z as $r^{2|\ell|}$, while a self-similar argument:

$$\chi = \big[(\omega_f-\omega_b)t-(k_f+k_b)z+2\ell\theta\big], \quad (8)$$

keeps the maxima of intensity at the 2ℓ collocated helices separated from each other by $\lambda/2$ interval (Fig. 1). The azimuthal term $2\ell\theta$ appears due to phase-conjugation $\mathbf{E}_b \sim \mathbf{E}_f{}^*$. Thus we have the following strict correspondence between the *roll* interference pattern (2) and the helical interference pattern (7): the frequency difference $\delta\omega = \omega_f-\omega_b$ is the cause of the translation of *rolls* with *group* velocity $V_z = (\omega_f-\omega_b)/(k_f+k_b)$ of the wavetrain, produced by a sum of the two counter-propagating beams $(\mathbf{E}_f+\mathbf{E}_b)$ [5]. The $\delta\omega$ is responsible also for the rotation of *helices* with angular velocity $\dot{\theta} = \delta\omega/2\ell$. The rotation is the cause of the *pitch* of helical interference maxima along z-axis. Consequently there exists a perfect mechanical analogy between the *solid body* rotation of the helix described by formula (7) and an Archimedean screw. Namely the positive $\delta\omega$ corresponds to the counter-clockwise rotation and this provides the *pitch* in positive z direction for *right* helices. On the other hand the negative $\delta\omega$ means clockwise rotation. In this case $(\delta\omega<0)$ the positive translation speed in z direction takes place for the *left*-handed helices. Evidently the change of the topological charge ℓ changes the direction of helix translation $\vec{V}_z$ due to alternation of the helix hand to the opposite one for a given $\delta\omega$.

This mechanical analogy is useful for the analysis of the cold atoms motion in the helical trap. The velocity vector of the condensate fragment trapped and perfectly collocated with intensity maxima has two components $\vec{V} = \vec{V}_z + \vec{V}_\theta$ (Fig. 1). The axial component is a *group* velocity $|\vec{V}_z| = (\omega_f-\omega_b)/(k_f+k_b)$ of the wavetrain, while the azimuthal component $|\vec{V}_\theta| = (\omega_f-\omega_b)\cdot D_0$ is of kinematic nature.

The electromagnetic orbital angular momentum inside LG beam waist volume $V \cong \pi D_0^2 z_R$ located near $z=0$ plane within Rayleigh range $|z| < z_R$ is the expectation value of the angular momentum operator $\hat{L}_z = -i\hbar[\vec{r}\times\nabla] = -i\hbar\frac{\partial}{\partial\theta}$ [24]:

$$\begin{aligned}\langle L_z\rangle_{(f,b)} &= \left\langle \Psi^{\ell}_{(f,b)}\middle|\hat{L}_z\middle|\Psi^{\ell}_{(f,b)}\right\rangle \\ &= 2\epsilon_0\int_V \left(E^{+}_{(f,b)}\right)^{*}\left(-i\hbar[\vec{r}\times\nabla]E^{+}_{(f,b)}\right)d^3\vec{r} \\ &= 2\epsilon_0\int \left(E^{+}_{(f,b)}\right)^{*}\left(-i\hbar\frac{\partial}{\partial\theta}E^{+}_{(f,b)}\right)r\,dr\cdot d\theta\,dz \\ &\simeq \pm\ell\hbar\frac{I_{(f,b)}V}{\hbar\omega_{(f,b)}c},\end{aligned} \tag{9}$$

where $I_{(f,b)} = \epsilon_0 c|\mathbf{E}_{(f,b)}|^2$ is the light intensity, $\Psi^{\ell}_{(f,b)} = \sqrt{2\epsilon_0}\times E^{+}_{(f,b)}(z,r,\theta,t)$ are the macroscopic wavefunctions of a single photon inside a forward or backward beam (5) with the winding number ℓ, E^{+} means the positive frequency components in $E(\vec{r},t)$ spectrum. The square modulus $|\Psi^{\ell}_{(f,b)}|^2$ is a probability density of the photon detection which is proportional to the energy density of classical wave [24]. In this particular paraxial case the spin–orbit coupling [25] is small enough and the angular momentum of the photon is exactly decoupled to the spin and the orbital component: $\hat{J} = \hat{S} + \hat{L}$. The linear momentum expectation values for the forward and backward LG are as follows:

$$\begin{aligned}\langle P_z\rangle_{(f,b)} &= \left\langle \Psi^{\ell}_{(f,b)}\middle|\hat{P}\middle|\Psi^{\ell}_{(f,b)}\right\rangle \\ &= 2\epsilon_0\int \left(E^{+}_{(f,b)}\right)^{*}\left(-i\hbar\frac{\partial}{\partial z}E^{+}_{(f,b)}\right)d^3\vec{r} \\ &\simeq \pm\hbar k_{(f,b)}\frac{I_{(f,b)}V}{\hbar\omega_{(f,b)}c}.\end{aligned} \tag{10}$$

The ratio of the angular and linear momenta is $L_z/P_z \sim \ell c/\omega_{(f,b)}$ [25]. The angular and linear momenta of the composite wavetrains (6) and (7) (Fig. 1) are:

$$\begin{aligned}\langle L_z\rangle_{(f+b)} &= \left\langle \Psi^{\ell}_{f} + \Psi^{\pm\ell}_{b}\middle|\hat{L}_z\middle|\Psi^{\ell}_{f} + \Psi^{\pm\ell}_{b}\right\rangle \simeq (\ell\hbar \pm \ell\hbar)\frac{I_{(f,b)}V}{\hbar\omega_{(f,b)}c}, \\ \langle P_z\rangle_{(f+b)} &= \left\langle \Psi^{\ell}_{f} + \Psi^{\pm\ell}_{b}\middle|\hat{P}\middle|\Psi^{\ell}_{f} + \Psi^{\pm\ell}_{b}\right\rangle \simeq (\hbar k_f - \hbar k_b)\frac{I_{(f,b)}V}{\hbar\omega_{(f,b)}c},\end{aligned} \tag{11}$$

where the upper sign in $\pm$ corresponds to reflection from conventional mirror while the bottom sign stands for the reflection from PC-mirror with alternation of the photon angular momentum.

The simplest conceivable configuration of linear PCM composed of plane mirrors, wavefront curvature compensating lenses and beam splitters is described in [27,23]. The goal of proposed setup is to counter-direct the split LG beams. The four reflections are the necessary minimum. The case is that the incidence angles much above 45 degrees will distort both polarization and spatial structure of LG. In addition a small sliding of a beam along the reflecting surface [26] may occur when mirror is tilted with respect to the LG propagation axis. The evident physical restriction on this *loop* setup is to keep the path difference ΔL of the counter directed LG smaller than coherence length of trapping laser field ($\Delta L \ll c\cdot\tau_{coh}$) [27]. The small frequency shift $\delta\omega \approx 2\pi\cdot 10^{-(1-3)}$ rad/s required to cause the helix rotation [11] might be induced by a frequency ramp [5] or via rotational Doppler shift which appears due to rotation of the half-wavelength plate [28] or Dove prism [29].

3. Cold ensemble density and velocity field in the helical trap

Consider a bosonic cloud prepared in an elongated trap [5] and suddenly released afterwards. The well elaborated experimental procedure is to impose a periodic optical potential to study the Bloch oscillations, macroscopic Landau–Zener tunneling and Josephson effects [4,6]. In our case the imposed optical potential is a *helical* one:

$$\begin{aligned}V_{opt}(z,r,\theta,t) &= -\frac{\mathrm{Re}[\alpha(\omega)]}{2\epsilon_0 c}I_{tw}(z,r,\theta,t), \\ \alpha(\omega) &= 6\pi\epsilon_0 c^3\frac{\Gamma/{\omega_0}^2}{(\omega_0^2-\omega^2-i(\omega^3/\omega_0^2)\Gamma)},\end{aligned} \tag{12}$$

where $\alpha(\omega)$ is the polarizability of atom, which is real, i.e. $\alpha(\omega)\approx \mathrm{Re}[\alpha]$ at large detunings from resonance $\omega-\omega_0$, $\Gamma = e^2{\omega_0}^2/6\pi\epsilon_0 m_e c^3$ is classical damping rate via radiative energy loss, m_e is electron mass [3]. The GPE for wavefunction Ψ of ensemble confined by V_{opt} is:

$$i\hbar\frac{\partial\Psi(\vec{r},t)}{\partial t} = -\frac{\hbar^2}{2m}\Delta\Psi + V_{opt}\Psi + \frac{4\pi\hbar^2 a_s(\vec{B})}{m}|\Psi|^2\Psi, \tag{13}$$

with $a_s(\vec{B}) = a_{bg}(1+\Delta_B/(|\vec{B}|-B_F))$ magnetic field dependent *s-wave* scattering length, where a_{bg} is background value of a_s, B_F and Δ_B are the Feshbach magnetic induction and resonance width respectively.

Consider the sufficiently large number of trapped atoms ($N \cong 10^{6-12}$). Then quantum pressure term following from the uncertainty principle is small ($\hbar^2\Delta\Psi/2m \sim 0$) compared to the optical trapping and interaction terms [4]:

$$\frac{E_{int}}{E_{kin}} \cong \frac{N\cdot a_{bg}}{a_{\mathbf{ho}}}, \tag{14}$$

where $a_{\mathbf{ho}} \cong \sqrt{\hbar/m\omega_z}$ is the "harmonic oscillator width" [4]. The ratio E_{int}/E_{kin} (14) is much more than unity for the most of the near infrared lasers $\lambda = 0.8$–1.5 μm, under the standard focusing requirement $D_0 \sim 10$–100 μm and when $a_s(\vec{B})$ is tuned in the range $\cong 1$–100 nm via Feshbach resonance. For the mid-infrared trapping at CO_2 lasing wavelength $\lambda = 10.6$ μm the kinetic energy term $E_{kin} = 2\hbar^2/m\lambda^2$ is about 100 times smaller. The optical dipole trapping energy E_{dipole} is:

$$\begin{aligned}E_{dipole} &\cong N\cdot V_{opt} \cong -\frac{\vec{p}\cdot\vec{E}}{2} \cong \frac{-\alpha\vec{E}^2 N}{2} \\ &\cong \frac{-\alpha I_{tw}N}{2\epsilon_0 c} = \frac{-e^2 I_{tw}N}{m_e\Delta\omega^2 2\epsilon_0 c}, \quad \Delta\omega = \omega_{f,b}-\omega_0\end{aligned} \tag{15}$$

where I_{tw} is the optical intensity of trapping beams [3]. Hence one might expect that a Thomas–Fermi approximation (TFA) is adequate in our case when interaction is repulsive $a_s > 0$ [4].

When inhomogeneous ensemble is considered in the thermodynamic limit ($N\to\infty$) the local density approximation for chemical potential is used $\mu(r) = \mu_{local}[\rho(\vec{r})] + V_{opt}(\vec{r})$ [4]. Let us consider the following TFA wavefunction in the vicinity of the LG beam waist (i.e. within Rayleigh range $|z| < z_R$):

$$\Psi_{fun} = \Phi(r)\exp\left[-\frac{i\mu(r)t}{\hbar} + i\Phi(r)^2\sin(\delta\omega t - 2k_z z + 2\ell\theta)\right], \tag{16}$$

where the local r-dependent chemical potential $\mu(r)$ is:

$$\begin{aligned}&\mu(r) = 4\pi\hbar^2 a_s\Phi(r)^2/m; \qquad I_{tw} = 2\epsilon_0 c|\mathbf{E}_{(f,b)}|^2; \\ &\Phi(r)^2 = \exp\left(-2r^2/D_0^2\right)\cdot(r/D_0)^{2|\ell|}\cdot\frac{\alpha(\omega)I_{tw}}{2\epsilon_0 c\cdot\hbar\cdot\delta\omega}.\end{aligned} \tag{17}$$

The wavefunction (16) is normalizable and fits the GPE by substitution. This TFA density of atoms $\rho_{fun}(z,r,\theta,t) = |\Psi_{fun}|^2 \sim \exp(-2(r/D_0)^2)/(r/D_0)^{2|\ell|}$ is (z,t)-independent "funnel" collocated with the optical helix $I_{tw}(z,r,\theta,t)$. The phase modulation of Ψ_{fun} has a maximum near the density maximum $\rho_{fun}(z,r,\theta,t)$, sinusoidal dependence on azimuthal angle θ and decreases down to zero on LG axis and outside the LG waist. Noteworthy $\arg[\Psi_{fun}]$ is a multiply valued function of θ. Hence this solution is of restricted interest. It may be used for evaluations of the thermodynamical parameters of the cold ensemble with $|\Psi_{fun}|^2$ density [4].

The other solution for dilute Bose gas (e.g. $N \sim 10^6$) is obtained in the TFA for r-independent chemical potential $\mu(\vec{r}) = \text{const}$. The mean field wavefunction here Ψ_h is a sum of the two phase-conjugated vortices with the opposite angular momenta $\pm\hbar\ell$:

$$\begin{aligned}\Psi_h(z,r,\theta,t) &= \Psi_\ell(z,r,\theta,t) + \Psi_{-\ell}(z,r,\theta,t)\\ &\cong \Psi_{\pm\ell}(z=0)\cdot\frac{(r/D_0)^{|\ell|}}{1+z^2/z_R^2}\exp\left[-\frac{r^2}{D_0{}^2(1+iz/z_R)}\right]\\ &\times\left\{\frac{\exp[-\frac{i\mu_f t}{\hbar}+ik_f z+i\ell\theta]}{(1+iz/z_R)}\right.\\ &\left.+\frac{\exp[-\frac{i\mu_b t}{\hbar}-ik_b z-i\ell\theta]}{(1+iz/z_R)}\right\},\end{aligned} \tag{18}$$

where the difference of the partial chemical potentials $(\mu_f - \mu_b)$, associated with the each of "counter-propagating" wavefunctions Ψ_ℓ, $\Psi_{-\ell}$ is adjusted to the frequency difference of counter-propagating optical fields $(\mu_f - \mu_b)/\hbar = \delta\omega = \omega_f - \omega_b$. The substitution of this TFA wavefunction into GPE gives the following link for parameters:

$$\begin{aligned}&\mu - \frac{\alpha(\omega)I_{tw}(0)\cdot[1+\cos(\delta\omega t+2kz\pm2\ell\theta)]}{2\epsilon_0 c\cdot g(1+z^2/z_R^2)}(r/D_0)^{2|\ell|}\\ &\times\exp\left[-\frac{2r^2}{D_0{}^2(1+z^2/z_R^2)}\right] = \rho_h(z,r,\theta,t),\end{aligned} \tag{19}$$

where $k = k_f \cong k_b$, $\mu = \mu_f \approx \mu_b$ is a constant (z, r, θ, t-independent) value of chemical potential, $g = 4\pi\hbar^2 a_s(\vec{B})/m$ is the interaction parameter. This is the quasiclassical restriction imposed on a homogeneity of chemical potential of the system in an external field V_{opt} [4]. In accordance to this solution the density of the cold atomic ensemble $\rho_h(z,r,\theta,t)$ is perfectly correlated with the rotating optical helix potential $I_{tw}(z,r,\theta,t)$ as depicted at Fig. 1. The density ρ_h rotates as a "solid body". The speed of the axial translation is $V_z = \lambda\cdot\delta\omega/4\pi$.

Apart from TF approximation the truly exact solution with nonzero kinetic energy exists $\Psi_{ex} = \Psi_f + \Psi_b$. It is also a superposition of the two counter propagating *paraxial* matter waves Ψ_f and Ψ_b. Let us reduce GPE (13) to the *paraxial* form relevant to highly elongated geometry, as a *helical* one in our case:

$$\begin{aligned}i\hbar\frac{\partial\Psi_{(f,b)}}{\partial t} &= -\frac{\hbar^2}{2m}\Delta_\perp\Psi_{(f,b)} - i\frac{2k_{(f,b)}\hbar^2}{2m}\frac{\partial\Psi_{(f,b)}}{\partial z} + V_{opt}\Psi_{(f,b)}\\ &+\frac{\hbar^2}{2m}k^2{}_{(f,b)}\Psi_{(f,b)} + g|\Psi_f+\Psi_b|^2\Psi_{(f,b)}.\end{aligned} \tag{20}$$

The perfect mutual cancellation of trapping and interaction terms:

$$-V_{opt}(z,r,\theta,t)\Psi_{(f,b)} = g|\Psi_f+\Psi_b|^2\Psi_{(f,b)}, \tag{21}$$

occurs when nonlinear defocussing due to positive scattering length a_s is compensated by attraction to intensity maxima caused by red detuning. Taking again the exact helical solution of (20) as a superposition of the two counter-propagating vortices:

$$\begin{aligned}\Psi_{ex}(z,r,\theta,t) &= \Psi_f(z,r,\theta,t) + \Psi_b(z,r,\theta,t)\\ &\cong \tilde{\Psi}_f\cdot\exp\left[-\frac{i\mu_f t}{\hbar}+ik_f z\right]\\ &+\tilde{\Psi}_b\cdot\exp\left[-\frac{i\mu_b t}{\hbar}-ik_b z\right],\end{aligned} \tag{22}$$

and under the natural assumptions:

$$k_{(f,b)}\partial\tilde{\Psi}_{(f,b)}/\partial z \gg \partial^2\tilde{\Psi}_{(f,b)}/\partial z^2, \tag{23}$$

two following equations for counter propagating and counter rotating matter waves $\tilde{\Psi}_f$ and $\tilde{\Psi}_b$ are valid:

$$i2k_{(f,b)}\frac{\partial\tilde{\Psi}_{(f,b)}}{\partial z} + \Delta_\perp\tilde{\Psi}_{(f,b)} - \left(k^2_{(f,b)} + \frac{2m\mu_{(f,b)}}{\hbar^2}\right)\Psi_{(f,b)} = 0, \tag{24}$$

which have the vortex solutions with charge ℓ for the $\tilde{\Psi}_{f,b}(z,r,\theta)$ with initial condition at $z=0$ equals $\tilde{\Psi}_0$:

$$\tilde{\Psi}_{(f,b)} \sim \frac{\tilde{\Psi}_0\cdot(r/D_0)^{|\ell|}\cdot\exp[-\frac{r^2}{D_0{}^2(1+iz/z_R)}\pm i\ell\theta]}{(1+iz/z_R)}. \tag{25}$$

The issues of dynamical stability of (22) with respect to small perturbations and thermodynamical stability from the point of view of least energy arguments deserve a further careful analysis and will be published elsewhere. For example transformation to the reference frame rotating with angular velocity $\Omega = \delta\omega/2\ell$ synchronously with trapping helix leads to equation [4,9,10]:

$$\begin{aligned}&i\hbar\frac{\partial\Psi}{\partial t} = -\frac{\hbar^2}{2m}\Delta\Psi + \tilde{V}_{opt}(z,r,\theta)\Psi + g|\Psi|^2\Psi - \Omega\hat{L}_z\Psi,\\ &\tilde{V}_{opt} \sim r^{2|\ell|}\exp\left(\frac{-2r^2}{D_0^2(1+z^2/k^2D_0^4)}\right)\left[1+\cos(2kz+2\ell\theta)\right],\end{aligned} \tag{26}$$

where stationary solutions for the diluted ($\mu = \text{const}$) ensemble $\Psi = \Phi(z,r,\theta)\exp(-i\mu t/\hbar)$ are given by:

$$\mu\Phi = -\frac{\hbar^2}{2m}\Delta\Phi + \tilde{V}_{opt}(z,r,\theta)\Phi + g|\Phi|^2\Phi + \Omega i\hbar\frac{\partial\Phi}{\partial\theta}. \tag{27}$$

4. Macroscopic observables

The helical solutions composed of the counter propagating free space LG wavefunctions apparently fit the continuity equation and have realistic field of velocities. In addition to the ensemble density $\rho(\vec{r},t)$ obtained above in TFA the structure of velocity field $\vec{V}(\vec{r},t)$ is a consequence of the complex geometry of the helical wavetrain which requires the perfect adjustment of the phase fronts achieved by phase-conjugation of colliding vortices. The one possible application of (18), (22) might be in using them as variational ansatz for emulation of GPE [30]. Nevertheless the explicit form of solutions Ψ_h (18), (22) offers a possibility to evaluate the macroscopic observables of the trapped ensemble. Helical wavetrain has nonzero momentum P_z (10):

$$\begin{aligned}\langle P_z\rangle_h &= \langle\Psi_h| - i\hbar\frac{\partial}{\partial z}|\Psi_h\rangle = N\hbar(k_f - k_b)\\ \Leftarrow\quad &\hbar\int_V dV\exp(-r^2)r^{2|\ell|}\left[k_f - k_b + k_f\exp(i\chi)\right.\\ &\left.-k_b\exp(-i\chi)\right],\end{aligned} \tag{28}$$

and easily calculated angular momentum L_z (9):

$$\langle L_z\rangle_h = \langle\Psi_h| - i\hbar\frac{\partial}{\partial\theta}|\Psi_h\rangle = N\ell\hbar(1\mp 1)$$
$$\Leftarrow \quad \hbar\int_V dV\,\exp\bigl(-r^2\bigr)r^{2|\ell|}\bigl[1\mp 1+\exp(i\chi)\mp\exp(-i\chi)\bigr], \tag{29}$$

due to the apparent identity $\int_0^{2\pi}\sin(\chi)\,d\theta = 0$. The upper $\mp$ sign in (29) corresponds to counter directed angular momenta and helical interference pattern (7), while bottom $\mp$ sign corresponds to the toroidal optical interference pattern (6).

The same expectation values $\langle P_z\rangle_{ex} = N\hbar(k_f - k_b)$ and $\langle L_z\rangle_{ex} = N\ell\hbar(1\mp 1)$ has exact wavefunction Ψ_{ex} (22). Quantum mechanically this happens because the wavefunction in both cases is a superposition of the two partial matter waves Ψ_f and Ψ_b in (22) (or Ψ_ℓ and $\Psi_{-\ell}$ in (18)) having opposite and quantized (i.e. equal to $\pm\ell\hbar$) mutually subtracted angular momenta. This means also that helical optical wavetrain (7) contains OAM of exactly $0\times\ell\hbar$ per photon, while toroidal wavetrain (6) contains $2\ell\hbar$ per photon (11) as shown in Section 2.

This feature looks seemingly counter intuitively from the point of view of classical hydrodynamics, but the similar results on vanishing of the moment of inertia for purely superfluid ensemble were summarized in [4]. Namely the density of atomic ensemble $\rho_h = |\Psi_{h,ex}|^2$ rotates as a *solid body* and one might expect that ρ_h to have classically the angular momentum $L_{class} = I_{zz}\cdot\delta\omega/2\ell$, where I_{zz} is the moment of inertia of the helical *wire* located in LG beam waist with the density profile ρ_h [31]:

$$\begin{aligned} I_{zz} &= \int Nm|\Psi_{h,ex}|^2 r^2\,dV \\ &= Nm\int|\Psi_{h,ex}|^2 r^3\,dr\,d\theta\,dz \\ &\simeq\sim Nm\int\bigl(1+\cos\bigl(\delta\omega t+(k_f+k_b)z+2\ell\theta\bigr)\bigr)\cdot d\theta\,dz \\ &\quad\cdot\exp\bigl(-r^2/{D_0}^2\bigr)r^{2+2|\ell|}\cdot r\,dr \sim Nm{D_0}^2 Z_r. \end{aligned} \tag{30}$$

Nevertheless due to the *quantization* of the angular momentum in free space, the oppositely directed angular momenta cancel each other completely, because they have integer opposite values of $\pm\ell\hbar$ [32]. In $T\to 0$ limit [4] the net angular momentum of the helical wavetrains (18), (22) is zero because the superfluid component remains only. On the contrary, the linear momentum is *not* quantized in free space and this leads to nonzero net linear momentum P_z of the ensembles (18), (22), regardless to the mutual orientation of their OAMs. The net momentum P_z is small because of the smallness of the *group* velocity of the helical wavetrain $V_z = \delta\omega/(k_f + k_b)$. For example when frequency splitting $\delta\omega$ is induced by rotational Doppler effect [27,28], the speed of the axial translation of the helical density profiles (18), (22) $V_z\sim$ is several μm per second (several rotations of helix per second).

The else interesting physical consequences relevant to experiments with trapped quantum gas may be formulated from the point of view of the Landau criterion $|\vec{V}| > \epsilon(\vec{p})/|\vec{p}|$ for the appearance of elementary excitations (rotons) and superfluidity destruction, where $\epsilon(\vec{p})$ is the energy–momentum dispersion relation in the frame moving with superfluid. Following [18,22] consider the flow of quantum gas in a narrow helical channel with velocity $\vec{V} = \vec{V}_z + \vec{V}_\theta$. In the rest frame the momentum of excitation $\vec{p}$ must be opposite to the velocity of superfluid $\vec{V}$, because of the least energy constraint imposed upon excitation $\epsilon(\vec{p}) + \vec{p}\cdot\vec{V} < 0$. Thus $\epsilon(\vec{p}) - |\vec{p}|\cdot|\vec{V}| < 0$ and $|\vec{V}| > \epsilon(\vec{p})/|\vec{p}|$. Because in our case the only significant component of $\vec{V}$ is $V_\theta = \delta\omega D_0/2\ell$ the excitations with momentum $\vec{p}$ appear when:

$$\delta\omega_{crit}D_0 > 2\ell\cdot\epsilon(\vec{p})/|\vec{p}|. \tag{31}$$

The experimentally controllable detuning $\delta\omega$ of counter propagating waves ω_f and ω_b by rotational Doppler effect [27] which leads to the change the angular velocity of helix rotation makes possible to determine the critical velocity of superfluid, defined by contact point of roton minimum of $\epsilon(\vec{p})$ with the line $|\vec{p}|V_\theta$. The turbulent excitations (rotons) are assumed to appear due to ejection of superfluid across the trapping potential barrier owing to centrifugal force, rather than because of the roughness or the channel end [18,22].

5. Conclusion

The flow of the degenerate quantum gas in helical trap had been studied analytically in the framework of the Gross–Pitaevskii equation. The necessary conditions were formulated for the appearance of the helical Bose–Einstein condensate flows due to the Thomas–Fermi balance of the self-defocussing of condensate with positive scattering length a_s and "red"-detuned optical dipole potential. The minimal achievable ensemble temperature might be approximately evaluated as a recoil one $T_{recoil} = 4\cdot\hbar^2/(2m\lambda^2\cdot k_B)$ [17]. The possible experimental implementation of helical trapping is a sudden *switching on* of the helical potential after the condensate release from elongated optical trap in a way similar to switching of accelerated grating in Ref. [5].

The peculiarities of the cooling mechanisms in this helical configuration were not considered in the current work. But the helical interference pattern (see Fig. 1) geometry might reveal the new features of the well elaborated mechanisms as the Doppler cooling [33], polarization gradient cooling [17] or velocity selective population trapping [34]. The newly found loop and helical features of the optical speckle patterns [35,36] are also a promising trapping opportunities which may enlighten the features of the Anderson localization of cold atoms in **1D** and **3D** speckle patterns [37].

Noteworthy the similar helical geometry of the colliding LG optical vortices of picosecond duration with opposite angular momenta proposed recently for the plasma currents excitation via ponderomotive force [23]. As the plasma vortices are the sources of the axial magnetic fields, the superfluid motion in helical trapping environment (13) is to be associated with a so-called *artificial* magnetic fields [9,10].

Acknowledgement

The partial support of the Russian Fund for Basic Research through grant 08-02-01229 is acknowledged.

References

[1] S. Tung, V. Schweikhard, E.A. Cornell, Phys. Rev. Lett. 97 (2006) 240402.
[2] S. Tung, V. Schweikhard, E.A. Cornell, Phys. Rev. Lett. 99 (2007) 030401.
[3] R. Grimm, M. Weidemuller, Yu.B. Ovchinnikov, Adv. At. Mol. Opt. Phys. 42 (2000) 95.
[4] F. Dalfovo, S. Giorgini, S. Stringari, L.P. Pitaevskii, Rev. Mod. Phys. 71 (1999) 463.
[5] M. Cristiani, O. Morsch, J.H. Muller, D. Ciampini, E. Arimondo, Phys. Rev. A 65 (2002) 063612.
[6] O. Morsch, M. Oberthaler, Rev. Mod. Phys. 78 (2006) 179.
[7] Y.V. Kartashov, B.A. Malomed, L. Torner, Phys. Rev. A 75 (2007) 061602.
[8] H. Sakaguchi, B.A. Malomed, Phys. Rev. A 75 (2007) 013609.
[9] A.L. Fetter, Rev. Mod. Phys. 81 (2009) 647.
[10] H. Sakaguchi, B.A. Malomed, Phys. Rev. A 78 (2008) 063606.
[11] A.Yu. Okulov, J. Phys. B 41 (2008) 101001.
[12] K. Volke-Sepulveda, R. Jauregui, J. Phys. B 42 (2009) 085303.
[13] T. Puppe, I. Schuster, A. Grothe, A. Kubanek, K. Murr, P.W.H. Pinkse, G. Rempe, Phys. Rev. Lett. 99 (2007) 013002.
[14] E.R.I. Abraham, J. Tempere, J.T. Devreese, Phys. Rev. A 64 (2002) 023603.

[15] M. Bhattacharya, Opt. Commun. 279 (2007) 219.
[16] M. Woerdemann, C. Alpmann, C. Denz, Opt. Express 17 (2009) 22791.
[17] J. Dalibard, C. Cohen-Tannoudji, J. Opt. Soc. Am. B 6 (1989) 2023.
[18] I.M. Khalatnikov, An Introduction to the Theory of Superfluidity, Perseus Publishing, Cambridge, MA, 2000.
[19] B.Y. Zeldovich, N.F. Pilipetsky, V.V. Shkunov, Principles of Phase Conjugation, Springer-Verlag, Berlin, 1985, Chapter 2.
[20] N.G. Basov, I.G. Zubarev, A.B. Mironov, S.I. Mikhailov, A.Y. Okulov, JETP 52 (1980) 847.
[21] J. Leach, M.J. Padgett, S.M. Barnett, S. Franke-Arnold, J. Courtial, Phys. Rev. Lett. 88 (2002) 257901.
[22] R.P. Feynman, Statistical Mechanics, Benjamin, Reading, MA, 1972, Chapter 11.
[23] A.Yu. Okulov, Phys. Lett. A 374 (2010) 4523.
[24] J.E. Sipe, Phys. Rev. A 52 (1995) 1875.
[25] L. Allen, M.W. Beijersbergen, R.J.C. Spreeuw, J.P. Woerdman, Phys. Rev. A 45 (1992) 8185.
[26] K.Yu. Bliokh, Yu.P. Bliokh, Phys. Rev. Lett. 96 (2006) 073903.
[27] A.Yu. Okulov, J. Opt. Soc. Am. B 27 (2010) 2424.
[28] J. Arlt, M. MacDonald, L. Paterson, W. Sibbett, K. Volke-Sepulveda, K. Dholakia, Opt. Express 10 (19) (2002) 844.
[29] J. Courtial, D.A. Robertson, K. Dholakia, L. Allen, M.J. Padgett, Phys. Rev. Lett. 81 (1998) 4828.
[30] B.A. Malomed, Variational methods in nonlinear fiber optics and related fields, in: E. Wolf (Ed.), Progress in Optics, vol. 43, North Holland, Amsterdam, 2002, pp. 69–191.
[31] L.D. Landau, E.M. Lifshitz, Mechanics, Butterworth-Heinemann, Oxford, 1976.
[32] M.F. Andersen, C. Ryu, P. Clade, V. Natarajan, A. Vaziri, K. Helmerson, W.D. Phillips, Phys. Rev. Lett. 97 (2006) 170406.
[33] V.S. Letokhov, JETP Lett. 7 (1968) 272;
T.W. Hansch, A.L. Schawlow, Opt. Commun. 13 (1975) 68.
[34] A. Aspect, E. Arimondo, R. Kaiser, N. Vansteenkiste, C. Cohen-Tannoudji, Phys. Rev. Lett. 61 (1988) 826.
[35] M.R. Dennis, R.P. King, B. Jack, K. O'Holleran, M.J. Padgett, Nature Phys. 6 (2009) 118.
[36] A.Yu. Okulov, Phys. Rev. A 80 (2009) 013837.
[37] L. Fallani, C. Fort, M. Inguscio, Adv. At. Mol. Opt. Phys. 56 (2008) 119.